PROJECTILE X-RAY CROSS SECTIONS FOR FULLY STRIPPED FLUORINE IONS ON ARGON

by

EDWARD WILLIAM PETTUS JR.

B.S., Purdue University, 1971

A MASTER'S THESIS

submitted in partial fulfillment of the

requirements for the degree

MASTER OF SCIENCE

Department of Physics

KANSAS STATE UNIVERSITY
Manhattan, Kansas

1974

Approved by:

James R. Macdonald
Major Professor

TABLE OF CONTENTS

ILLEGIBLE DOCUMENT

THE FOLLOWING DOCUMENT(S) IS OF POOR LEGIBILITY IN THE ORIGINAL

THIS IS THE BEST COPY AVAILABLE

THIS BOOK
CONTAINS
NUMEROUS PAGES
WITH THE ORIGINAL
PRINTING BEING
SKEWED
DIFFERENTLY FROM
THE TOP OF THE
PAGE TO THE
BOTTOM.

THIS IS AS RECEIVED
FROM THE
CUSTOMER.

LIST OF TABLES AND PLATES

PLATES

I. Plot of x-ray yield as a function of target gas pressure in microns of Hg.

II. Branching percentages for the decay of a hydrogenlike system. All values are rounded to two significant digits and expressed as percentages.

III. A schematic diagram of the experimental beam line including the incident charge preparation equipment, the gas cell region and the charge spectrometer.

IV. The geometry for the determination of the solid angle correction factor. P_0, P_2 and P_3 are all points on the beam line, P_1 and P_5 are points defined by the limiting aperture through which the detector looks, and the circle is the active area of the detector. R connects an arbitrary point P on the detector to an arbitrary point Po on the beam line. The parameters defining the system are L, d, β and S_2.

V. Plot of Si(Li) detector efficiency as a function of energy for two different Beryllium window thicknesses (x).

VI. Sample spectrum showing yield plotted as a function of channel number.

VII. High resolution spectrum from the experiment by Macdonald et al.[21]

VIII. Sample plot of x-ray yield against detector channel number (a function of x-ray energy). The circles represent actual data points while the smooth line represents the fit to the data calculated by adding together four gaussian peaks.

IX. Plot of cross sections as a function of incident projectile energy. Points connected by a smooth line are hydrogenic x-ray production cross sections of fluorine projectiles measured in this paper. Points connected by the dashed line are single electron capture cross sections measured by Chaio[22]. Lines are drawn only to guide the eye. The solitary circle represents the x-ray production cross section calculated with the 2p-1s relative intensity equal to 1.5.

X. Sample plot of x-ray yield against detector channel number (a function of x-ray energy). The circles represent actual data points while the smooth line represents the fit to the data calculated by adding together four gaussian peaks. The low shoulder was not possible to fit without changing the relative intensities.

Introduction

Collisions between atoms and highly charged ions travelling at keV energies and above often result in inner shell vacancy production in both the target and the projectile. There are at least three ways to produce such inner shell vacancies: collision induced inner shell excitation or ionization which is reviewed by Garcia, Fortner, and Kavanagh[1], electron promotion which was suggested by Fano and Lichten[2], and electron capture which is well covered by Betz[3]. Since these vacancies are filled by higher level electrons decaying by either radiative (x ray producing) or Auger type transitions, the collision process can be studied by observing the characteristic x-ray production cross sections. Theoretically calculated fluorescence yields (for example, those by McGuire[4]) can then be used to convert x-ray production cross sections to inner shell vacancy production cross sections (i.e., radiative plus Auger processes).

Over the past decade such collision induced x rays have been the subject of extensive study, with target x rays being the ones most commonly investigated. This thesis, however, is a study of hydrogenlike projectile x rays resulting from electron capture by fully stripped fluorine ions incident on an argon gas target.

Since in hydrogenic decay there are no other electrons to take part in Auger decay processes, the fluorescence yield for the system studied is unity. Furthermore, a bare fluorine ion initially has no electrons to undergo excitation or promotion so that electron capture to excited states becomes the only vacancy producing process. Although electron capture has been studied by many researchers[3,5-7] most of this work has con-

cerned capture to the ground state. By using a variation of the Brinkman-Kramers approximation, Nikolaev has developed a formula for electron capture by protons in any target. However, currently there is very little literature on capture to excited states[3,6-9] for heavy ion projectiles on heavy targets. In general, there have been relatively few studies of x-ray production in projectiles undergoing heavy ion collisions of any kind; a brief summary of what has been done follows.

The lifetimes of various states have been studied by measuring the intensity of collision-induced projectile x rays as a function of time of flight by sampling the x ray intensity along the beam at selected distances from the collision point. A deviation from normal exponential decay in the intensity time curve has been used to indicate long-lived states. Using a proportional counter with a Bragg cyrstal spectrometer in beam foil experiments, Sellin et al.[10] noticed a long-lived component in some of their exponential decay curves hinting at metastable states with inner-shell vacancies in oxygen ions. With a Si(Li) detector Schmieder & Marrus[11] have measured lifetimes in He-like Ar while Cocke et al.[12] have measured x ray metastable states of Cl. Richard et al.[13] have used a high resolution crystal spectrometer to study fluorine metastable x rays using the beam foil procedure.

Researchers have also investigated the dependence of projectile x ray production cross sections on target atomic number (Z_2). Kavanagh et al.[14] measured copper projectile L x-ray production cross sections and noticed a strong cyclic dependence on Z_2. They suggested a dramatic influence on vacancy production depending on the relative spacing of levels

between the target and projectile. In experiments with Cl projectiles on gas targets by Winters et al.[15] the x ray production cross sections exhibited a nonmonotonic dependence on the target atomic number. Kubo, Jundt, and Purser[16] studied projectile K x-ray production cross sections in nickel and bromine and suggested that processes involving promotion of 2p vacancies are significant as high as 1.5 MeV/amu. Datz et al.[17] studied iodine L x rays for collisions of iodine on various targets and noticed a variation in the formation of vacancies in the $2p_{1/2}$, $2p_{3/2}$, and $2s_{1/2}$ subshells with slight changes in Z_2. Woods et al.[18] observed Cl projectile x rays under high resolution and observed a peaking effect in the ratio of double K shell to single K shell vacancy production as a function of Z_2. A molecular orbital mechanism was suggested to promote both K shell electrons to higher levels.

Both total and differential projectile x ray cross sections have been measured as a function of impact parameter. Stein et al.[19] measured L x rays produced in I on Te collisions in coincidence with the scattered iodine ions. They observed a maximum L x-ray production for impact parameters comparable to L shell radii. Cocke et al.[20] observed chlorine x rays in collisions involving Cl on Al, Ti, and Cu in coincidence with the scattered Cl ion. For comparable Z values in the Cl--Ti collisions as a function of impact parameter, the excitation probability shows an enhancement in magnitude and, in addition, an altered curve shape when compared to asymetric collisions. A promotion mechanism has also been suggested as being responsible for this difference.

Recently Macdonald et al.[21] used a high resolution crystal spectrometer to study the relative distribution of highly charged fluorine projectile x rays when 7, 8 and 9+ fluorine ions were incident on argon gas. They measured the relative intensities of transitions in fluorine ions and showed the importance of electron exchange processes in collisions in which inner shell excitation occurs.

In the high resolution experiment of Macdonald et al.[21], the hydrogenic fluorine x ray lines were resolved and their relative intensities were measured, but the absolute cross sections for x ray production could not be determined since the absolute efficiency of the high resolution detector was not known. The present work is an experiment designed to measure the absolute total cross section for hydrogenic x ray production by fluorine 9+ ions incident on argon gas. Since the incident beam is fully stripped fluorine, hydrogenic x rays can only occur as a result of single electron capture to excited states. Thus, this experiment allows a comparison between the total cross section for capture to all excited states but the 2s and capture to all states as measured by Chiao.[22]

The cross sections reported here were measured using a thin gas target. Although a gas target is much harder to set up and use than a solid target, single collision conditions for charge exchange are available with a gas target. This is shown by the linearity of the x ray yield against pressure curve in Plate I. Both the initial and final states of the projectile ion can be determined in such collisions with gas targets. In addition, with a thin gas target, stopping power formulas are unnecessary in the

analysis, and self absorption by the target gas of the x rays is negligible. Finally one can obtain a continuous range of target thicknesses by changing the gas pressure.

Plate I

Plot of x-ray yield as a function of target gas pressure in microns of Hg.

Plate I

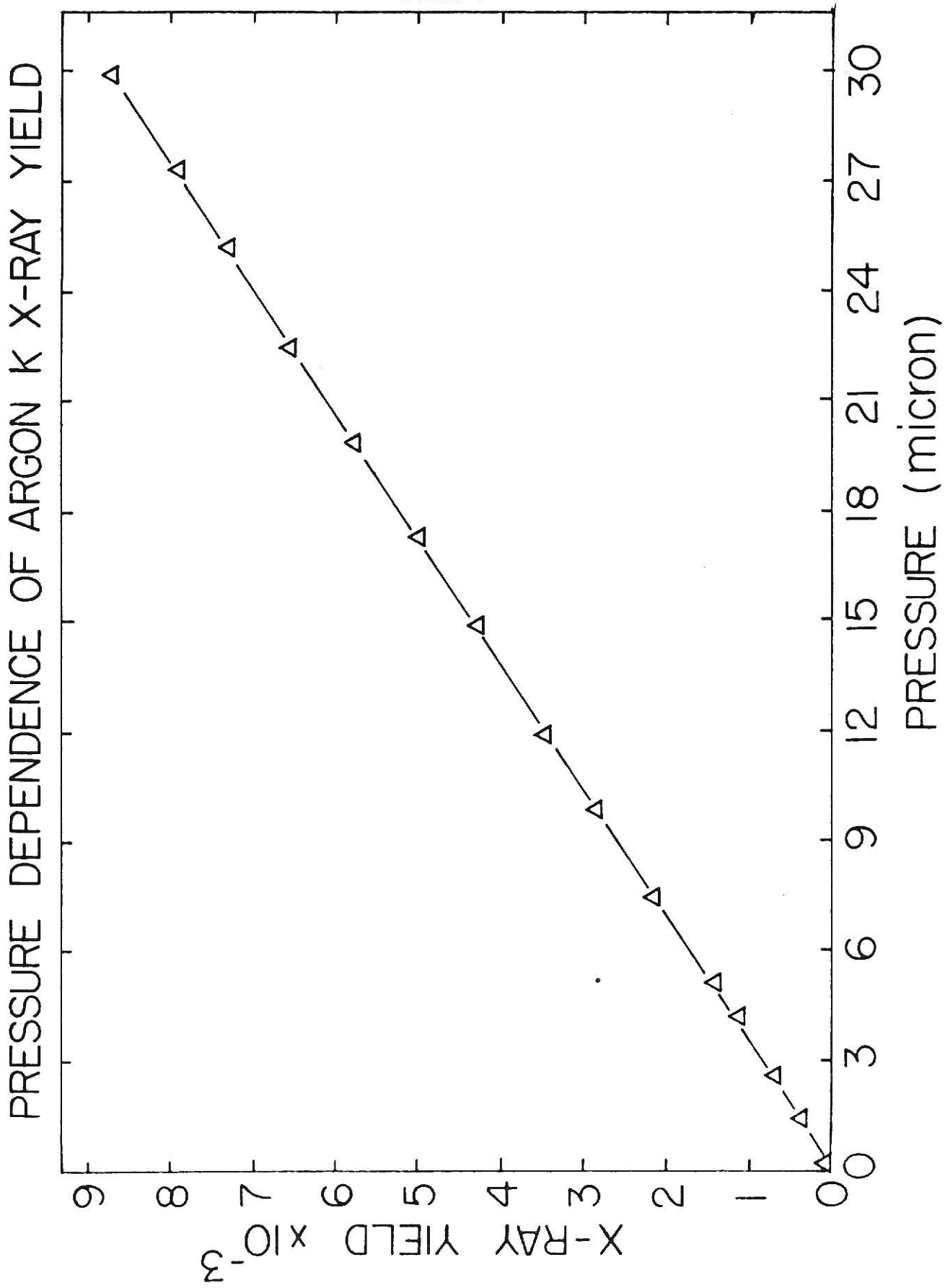
PRESSURE DEPENDENCE OF ARGON K X-RAY YIELD
X-RAY YIELD x10⁻³
0
1
2
3
4
5
6
7
8
9
0
3
6
9
12
15
18
21
24
27
30
PRESSURE (micron)

Theory

To produce projectile characteristic x rays, electrons must be able to decay down to innershell vacancies. These vacancies may be produced in several ways: 1) by collision induced innershell excitation or ionization, 2) by electron promotion to higher levels during a collision (thus creating a vacancy), or 3) by electron exchange or capture. For fully stripped projectiles where there are no electrons present to undergo excitation or promotion, electron capture into excited states is the only process.

Electron capture has been extensively studied for simple cases such as protons, helium ions, or hydrogen like ions passing through similarly light atoms.[7] Oppenheimer assumed capture into s states only and showed that alpha particles capture electrons from hydrogen-like atoms into excited states according to the relation:

$$\sigma_n = \sigma_1 / n^3 \quad (v >> v_o) \qquad (1$$

where n is the principal quantum number and v_o is equal to $e^2/\hbar$ or 2.2×10^8 cm/sec. Although there have been some improvements in the details of the calculation[8,23] it has been suggested[24] that Eqn. (1) is a useful approximation. In collision systems for which this estimate is correct, about 85% of the electrons captured are captured to ground state. For lower velocities (v=vo) Jackson and Schiff[25] and Schiff[26] have shown that capture into the 2p state is larger than into the 2s state. Omidvar[8] has suggested that for n sufficiently large, n electron capture is proportional to $1/n^2$. However, for capture by highly charged particles, the linear Stark splitting assumed by Omidvar is probably no longer linear

so that his calculations may not apply to this experiment.

For collisions involving partially stripped heavy ions and heavy targets there is very little information available. Bohr and Lindhard[27] estimate on general grounds that fast heavy ions capture electrons from heavy targets into modestly high excited states. Recently Dmitriev[6] offered indirect experimental evidence that electron capture in ions with $Z > 4$ is mainly to excited states. Experimentally, the electron capture cross sections to all states (including ground state) have been measured[22] for single electron capture. A comparison of these cross sections with those for capture to excited states are discussed in the present work.

No unfolding of the cascading process to obtain the excited state distribution produced by electron capture has been undertaken in this work as the solution cannot be uniquely found without a theoretical model of the distribution of capture to various substates of each shell. Depending upon which excited state the electron is captured to, there are a variety of decay modes resulting in a np-1s x ray transition. Plate II shows the branching percentages for a one electron fluorine ion calculated from the theoretical transition probabilities.[28]

Assuming that electrons can be captured to any level and so have any allowed combination of quantum numbers n and l, an equation can be written to combine the various branchings possible that would result in a particular x ray:

$$I_{np} = B_{1s}^{np} X_{np} + B_{1s}^{np} \sum X_{n'\ell'} \left[B_{n\ell}^{n'\ell'} + B_{n''\ell''}^{n'\ell'} B_{np}^{n''\ell''} + \ldots \right] \qquad (2$$

where I_{np} is the number of electrons making the transition from np-1s, X_{nl} is the number of electrons captured to state nl, $B_{nl}^{n'l'}$ is the branching

Plate II

Branching percentages for the decay of a hydrogenlike system. All values are rounded to two significant digits and expressed as percentages.

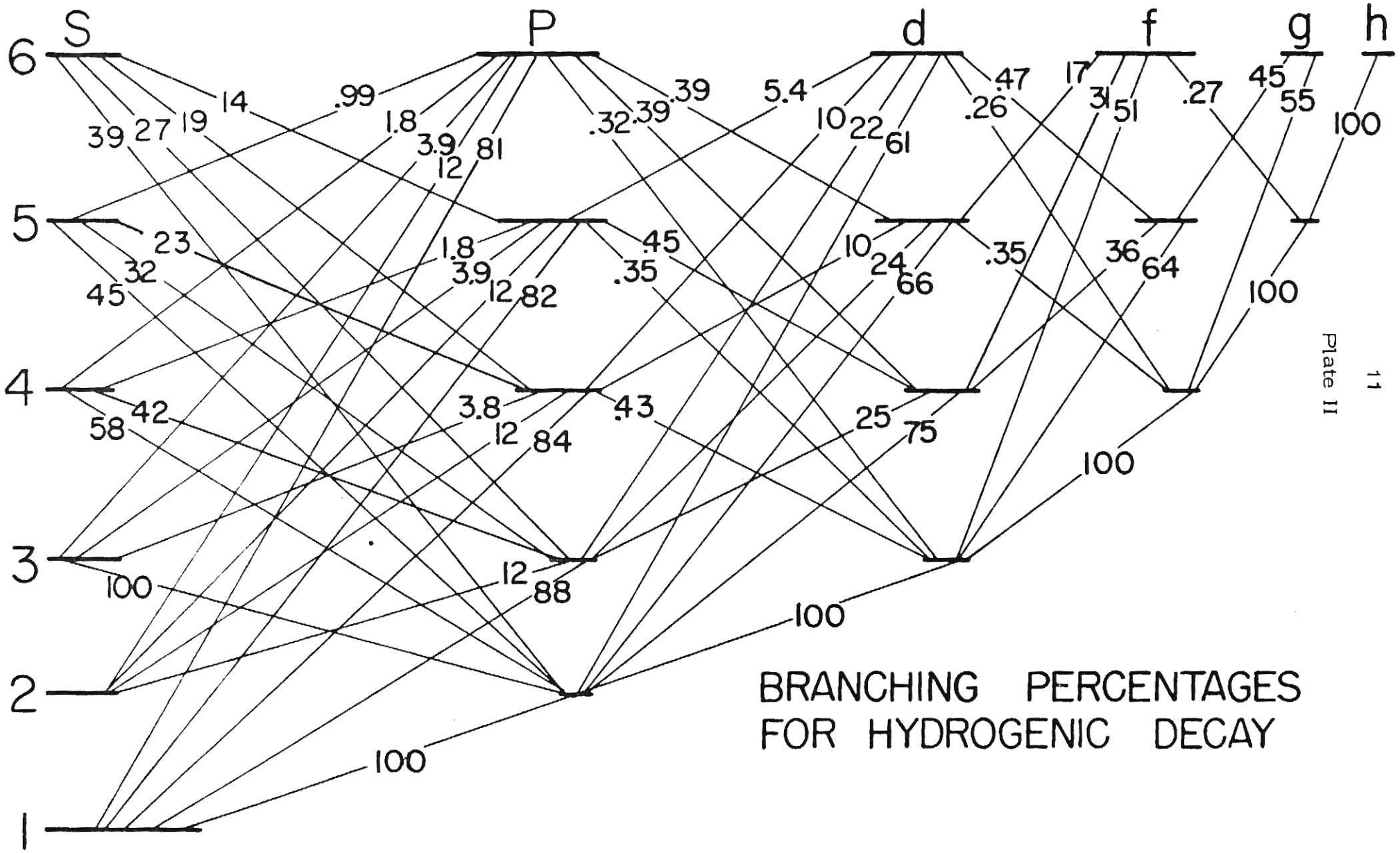
S
P
d
f
g
h
6
5
4
3
2
1
14
.99
39
27
19
1.8
3.9
12
81
.32
.39
.39
5.4
10
22
61
.47
.26
17
31
51
.27
45
55
100
23
45
32
1.8
3.9
12
82
.45
.35
10
24
66
.35
36
64
100
42
58
3.8
12
84
.43
25
75
100
100
12
88
100
100
BRANCHING PERCENTAGES
FOR HYDROGENIC DECAY

Plate II

fraction for the transition from n'l' to nl and the summation is taken over all n', l', n'',l''; ... (subject to selection rules) with np corresponding to the np-1s transition to be studied. The "X" on the right side of the equation are the unknowns while "I" can be experimentally determined using methods described later in this paper. Since there will be an equation for each different np-1s transition (I) while there are usually several "X" for each "I", there are clearly more unknowns than there are equations. Thus, using experimentally determined values for np-1s x ray transitions and branching equations such as Eqn. (2), it is not possible to solve for the relative distribution of capture to various states. However, in the future, when theoretical models for the distribution X_{nl} are available, equation (2) can be used to test the model with the results of this thesis.

Alternatively, one could assume a tentative model for the distribution of captured electrons and use the previous system of equations to test it. Although there is no well accepted model for heavy ions on heavy targets[3], several light ion-atom models can be tried and the results compared to the relative intensities from reference 21: 1.00, 0.26, 0.12, 0.08, (normalized to the 2p-1s transition intensity). Table I shows the results of three such models. Apparently none of these models is an adequate description of the capture process since in all three tests the relative intensities of the higher energy transitions were much smaller than the high energy intensities actually measured by experiment.[21]

The x-ray transitions for the system involve a hydrogenic decay scheme, and a Z_1-squared Lyman series formula gives the energies:

$$E = Z_1^2 (13.6\,eV)(1 - 1/n_i^2) \qquad (3$$

where Z_1 is the projectile atomic number and n_i is the quantum number of the initial state for the x ray transition np–1s (n_i=2,3,4,5,...). In this thesis, the x rays have been observed in a Si(Li) detector with approximately 150 eV resolution at ~ 1keV. Thus the separate lines have not been resolved experimentally, but a fitting procedure has been used to obtain the total spectral distribution and absolute intensity of the x rays.

Table I

Relative intensities of the first four x-ray lines for hydregenic decay in fluorine. Three electron capture models are tested against the relative intensities from the work by Macdonald et al.[21] The first model assumes a level distribution of $1/n^3$ with capture to s states only. The second model also assumes $1/n^3$ but the electrons are distributed over the l states proportionally to $2l+1$. The third model assumes $1/n^2$ with a $2l+1$ distribution.

Table I

	Measured Intensities	$1/n^3$ s only	$1/n^3$ 2l+1	$1/n^2$ 2l+1
2p-1s	1.00	1.00	1.00	1.00
3p-1s	0.26	0.10	0.09	0.11
4p-1s	0.12	0.01	0.02	0.03
5p-1s	0.08	0.002	0.007	0.01

Experimental Design

The fluorine projectiles for these experiments were accelerated by the Kansas State University Tandem Van de Graaff accelerator. The fluorine ions are accelerated up to the desired energy and then momentum analyzed by a 90^{o} magnet whose energy window is about 10 keV. The ions are then passed through a stripping foil which gives the beam a distribution of charge states all at one selected energy. A switching magnet selects out the fluorine 9+ ions to be used in this experiment. This ion beam is focused down the beam line where it is collimated by two adjustable tantalum slits before reaching the target gas cell. The gas cell is differentially pumped by three oil diffusion pumps. The beam line pressure was about 5×10^{-7} torr.

The target for this experiment was argon gas at pressures up to 5 or 6 microns of Hg and temperatures in the neighborhood of 20^{o} C. Target gas pressures were regulated by an MKS Baratron, type 90 capacitance Manometer, coupled to a Granville-Phillips 213 Automatic Pressure Controller. In addition to its factory calibration, the manometer was calibrated while on the gas cell by a GM-100A McLeod gauge which was itself calibrated at the National Bureau of Standards. The accuracy of the manometer was better than 10% at pressures between 1 micron and 1 torr. Since the detection system was sensitive to noise vibrations, the pressure controller was turned off during actual runs. The gas pressure was monitored during each run and allowed to vary, monotonically, to a maximum of 5%. In this experiment 1 to 20 na of beam were typically available at the entrance to the gas cell and about 30% of this passed into and through

the interaction region. By means of a series of Faraday cups within the cell, 100% transmission through the cell was guaranteed.

The gas cell, shown in Plate III, had four beam slits made of graphite to reduce x-ray background. Slit sizes were: s_1 = 1.0mm, s_2 = 1.5mm, s_3 = 2.5mm, s_4 = 3.0mm. Between s_1, s_2 and s_2, s_3 there were movable Faraday cups with -500V suppressor rings used to focus the beam through the slits. The beam was focused to insure 100% transmission between s_2 and s_4. This was a critical factor since cross section analysis requires knowledge of the number of ions passing through the interaction region of the gas cell with 100% transmission. The beam current was monitored behind s_4 in a large Faraday cup suppressed by a -500V suppressor ring and integrated by a Brookhaven current integrator. A retractable target holder was used inside the gas cell to support an ^{55}Fe x ray source and various solid targets to calibrate the x ray detector.

A charge spectrometer, consisting of a magnet and a position sensitive particle detector was mounted behind the last Faraday cup (see Plate III). The charge purity of the incident beam was measured to insure that the incident beam was better than 99% pure bare nuclei. Projectile final charge state distributions were measured so that the gas target thickness could be set to insure that less than 5% of the beam underwent charge exchange. In addition, the charge spectrometer was used to measure the cross section for single electron capture (summed over all states) for F^{9+} ions on argon[22].

The detection system consisted of a liquid nitrogen cooled Si(Li) detector[29] mounted in the gas cell at right angles to the beam line. The

Plate III

A schematic diagram of the experimental beam line including the incident charge preparation equipment, the gas cell region and the charge spectrometer.

Plate III

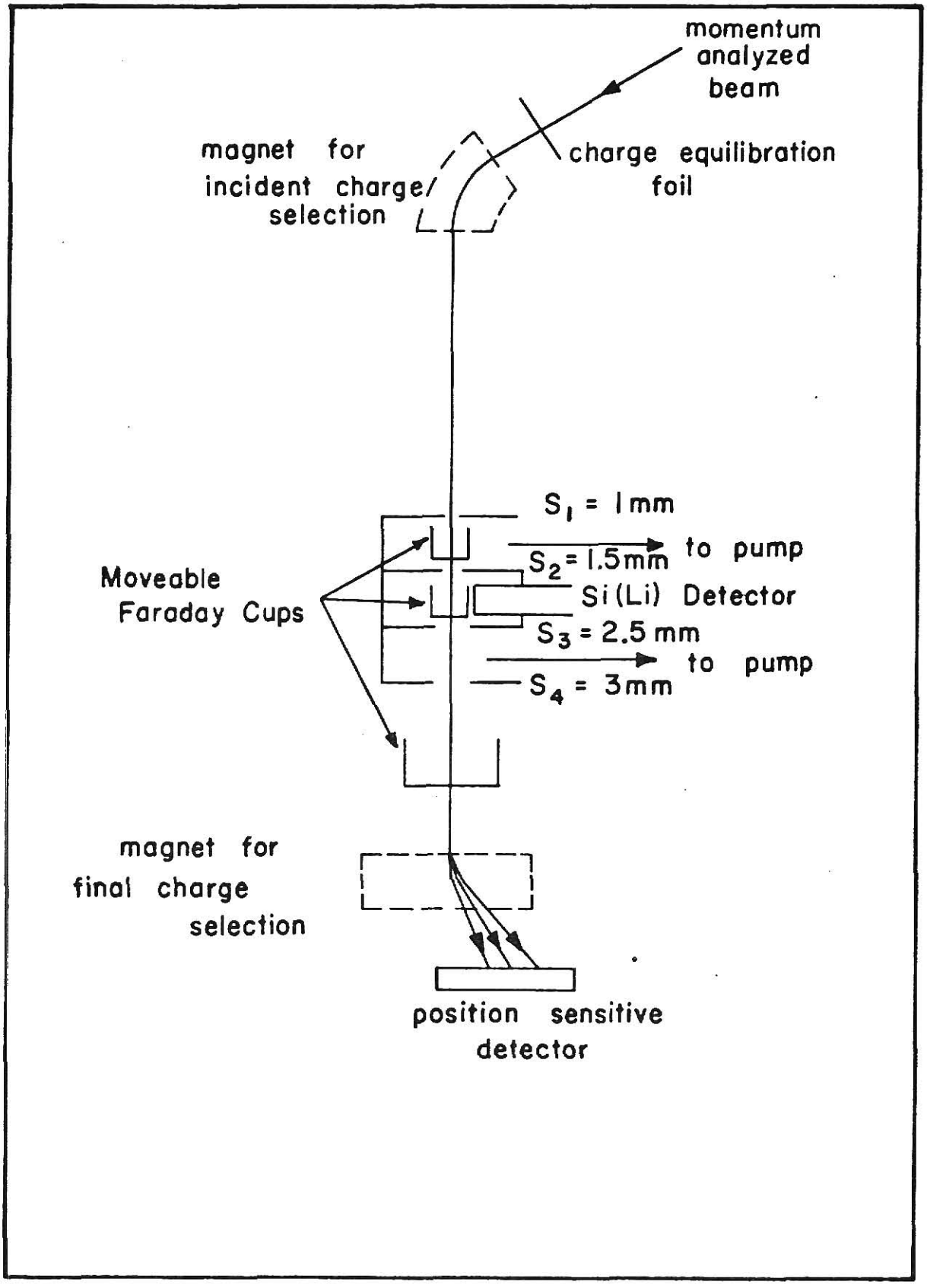
momentum analyzed beam
magnet for incident charge selection
charge equilibration foil
S_1 = 1mm
to pump
S_2 = 1.5mm
Moveable Faraday Cups
Si(Li) Detector
S_3 = 2.5 mm
to pump
S_4 = 3mm
magnet for final charge selection
position sensitive detector

detector had an active area of 80mm^2 and was maintained under separate vacuum by a .025mm beryllium window. The resolution was in the neighborhood of 200 eV FWHM at 6 keV photon energy.

In order to extract absolute cross sections from the observed x-ray intensities, the solid angle integrated over the interaction region ($\Omega\mathfrak{L}$) for the geometry of the detector-beam combination must be known. A first approximation can be made by multiplying the beam line interaction length ($\mathfrak{L}$) seen by the detector by the solid angle subtended by the detector area from an arbitrary point on the beam line. This would give

$$\Omega\mathfrak{L} = \left(\frac{a}{4\pi x^2}\right)\mathfrak{L} \qquad (4$$

where "a" is the detector active area and "x" is the distance from the detector to the beam line. However, this approximation ignores edge "shadow" effects which become important since the detector must be close to the beam line to optimize the counting statistics. Alternately, an exact analytical expression can be written for the solid angle in the form of a triple integral. Plate IV shows a diagram of the geometry. The solid angle at an arbitrary point P_o can be written as:

$$\Omega(P_o) = \iint \frac{r\,dr\,d\theta}{4\pi R^2}, \quad R^2 = (L+d)^2 + r^2 + \alpha^2 + 2\alpha r\sin\theta \qquad (5$$

Integrating over the entire interaction length $\mathfrak{L}$ gives:

$$\Omega\mathfrak{L} = \iiint \frac{r\,dr\,d\theta\,d\alpha}{4\pi R^2} \qquad (6$$

$$\Omega\mathfrak{L} = \frac{4}{4\pi}\int_0^{S_2} r\,dr \int_0^{\pi/2} d\theta \int_{-Y_2}^{Y_3} \frac{d\alpha}{(L+d)^2 + r^2 + (2r\sin\theta)\alpha + \alpha^2} \qquad (7$$

The third integral can be solved analytically using trigonometric identities to yield:

$$\int_{-Y_2}^{Y_3} \frac{d\alpha}{R^2} = \frac{1}{\sqrt{D}}\left[\tan^{-1}\frac{Y_3 + r\sin\theta}{\sqrt{D}} - \tan^{-1}\frac{-Y_2 + r\sin\theta}{\sqrt{D}}\right] \qquad (8$$

$$D = r^2\cos^2\theta + (L+d)^2$$

$$\int_{-Y_2}^{Y_3} \frac{d\alpha}{R^2} = \frac{1}{\sqrt{D}}\tan^{-1}\left[\frac{(Y_3 + Y_2)/\sqrt{D}}{1 + 1/D\{Y_3(-Y_2) + r^2\sin^2\theta + (Y_3 - Y_2)\, r\sin\theta\}}\right]$$

Expressions for y_3 and y_2 can be derived from Plate V:

$$X_1^2 + Y_1^2 = r^2 \qquad X_1 = r\cos\theta \qquad Y_1 = r\sin\theta$$

$$Y_4 = -Y_5 = \beta \qquad X_4 = X_5 \qquad S_1^2 = \beta^2 + X_4^2 = \beta^2 + X_5^2$$

$$\frac{X_1}{L+d} = \frac{X_4}{d} \qquad X_4 = \frac{X_1 d}{L+d} = \frac{d}{L+d} r\cos\theta = X_5 \qquad (9$$

$$\frac{\beta - Y_1}{L} = \frac{Y_2 - Y_1}{L+d} \qquad \frac{\beta + Y_1}{L} = \frac{Y_3 + Y_1}{L+d}$$

$$Y_2 = \left(\frac{L+d}{L}\right)\beta - \frac{rd}{L}\cos\theta \qquad Y_3 = \left(\frac{L+d}{L}\right)\beta + \frac{rd}{L}\cos\theta$$

Substituting these expressions for y_2 and y_3 and collecting terms we have:

$$\Omega\mathcal{I} = \frac{1}{\pi}\int_0^{S_2} r\,dr \int_0^{\pi/2} \frac{d\theta}{\sqrt{D}} \tan^{-1}\{f(r,\theta)\} \qquad (10$$

$$f(r,\theta) = \frac{2\beta[(L+d)/L]\sqrt{D}}{r^2 + (L+d)^2(1 - \beta^2/d^2) + \frac{2d}{L} r^2\sin^2\theta + \frac{d^2}{L^2} r^2\sin^2}$$

The following expression is then numerically integrated by computer:

$$\Omega\mathcal{I} \simeq \frac{\Delta r\,\Delta\theta}{\pi} \sum_{r=0}^{S_2} \sum_{\theta=0}^{\pi/2} \frac{r}{\sqrt{D}} \tan^{-1}\{f(r,\theta)\} \qquad (11$$

The result of .0208071 cm is the value for $\Omega\mathcal{I}$ computed from 50 increments for both r and θ. This was equal to the value obtained (to six significant digits) when only 10 increments were used for r and θ.

The x ray production cross section is given by the following equation:

$$\sigma_x = Y_T^c / N\, n'\, \Omega_T \qquad (12$$

Plate IV

The geometry for the determination of the solid angle correction factor. P_o, P_2, and P_3 are all points on the beam line, P_1 and P_5 are points defined by the limiting aperture through which the detector looks, and the circle is the active area of the detector. R connects an arbitrary point P_1 on the detector to an arbitrary point P_o on the beam line. The parameters defining the system are L, d, β, and S_2.

Plate IV

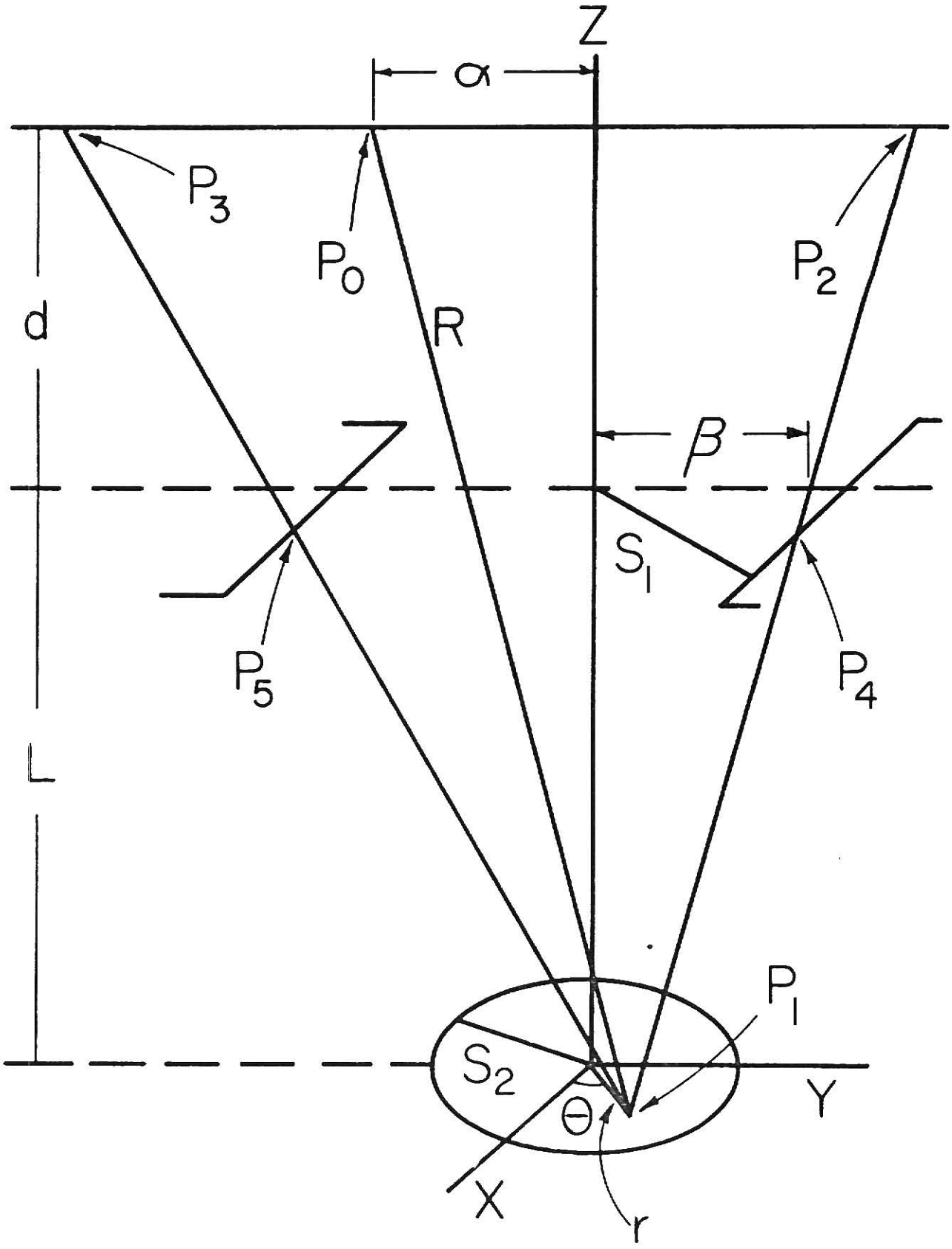

where Y_t^c is the total x-ray yield per micron of pressure corrected for the efficiency of the detector and the electronic dead time, n' is the number of target atoms per unit volume at 1 micron pressure and 20° C, N is the number of incident particles, and Ω_T is the solid angle integrated over the interaction length.

Since the experiment was conducted with a thin gas target, only single collision phenomena occur. The x-ray yield is linear with pressure and, as Plate I shows, the single collision assumption is good to much higher pressures than were used in this experiment. The corrected x-ray yield per micron of target gas pressure is obtained by plotting the number of x rays in a peak against the target pressure in microns of Hg. The method used to obtain the yield of x rays from the spectra will be discussed later. A least squares fitting routine[30] is used to calculate the required slope Y_t in x rays per micron and the result is divided by the efficiency of the detector at that particular energy.

For x rays below 1 keV in energy, absorption between the source and the detector is by far the most important factor in determining x-ray yields. For the x rays observed in this work from the transitions between one-electron fluorine states, over 90% of the x rays are absorbed. Since thin gas targets are used in this experiment, self absorption by the gas is negligible (less than .01%)[31]. The major absorption is due to the beryllium window with a smaller contribution from the gold and insensitive silicon layers of the detector.

At present there are no published experimental efficiency curves for Si(Li) detectors in the region of 1 keV and lower because of the extreme

sensitivity of efficiency to such factors as detector window thickness. However, a comparison of the available experimental efficiency curves[32,33] at much higher energies and theoretical calculations of such curves suggests that low energy efficiency curves might be obtained from theory. A large error is immediately introduced because the thicknesses of the absorbing layers are not accurately known. At energies between 0.5 and 1.0 keV the absorption is due primarily to the beryllium window so that the uncertainty in the gold and silicon layers becomes less important.

Initially an efficiency curve was calculated for the system assuming the following thicknesses: 0.025mm $\pm$ 20% Be, a dead layer equivalent of 0.1 microns Si at 6 keV as estimated by the manufacturer[29] and an average 20ug per cm^2 of Au. Absorption coefficients were taken from the work by W. J. Veigele[31]. The results are shown in Plate V as the solid line. The dominent feature in this curve is due to the beryllium window absorption with the transmission given approximately by:

$$\xi_{Be} = e^{-ax/E^3} \qquad (13$$

where x is the window thickness, E is the x-ray energy, and a is a constant representing the beryllium absorption coefficient. These calculations ignore the possibility of impurities in the beryllium. Although the specified purity from the manufacturer is better than 99.995% any impurities are of much larger atomic number and thus a source of systematic error which was not covered in this work.

A pulsed optical feedback preamplifier was used with the x ray detector so that a significant dead time occured during data accumulation and a correction was necessary for proper beam normalization. This was done

Plate V

Plot of Si(Li) detector efficiency as a function of energy for two different Beryllium window thicknesses (x).

Plate V

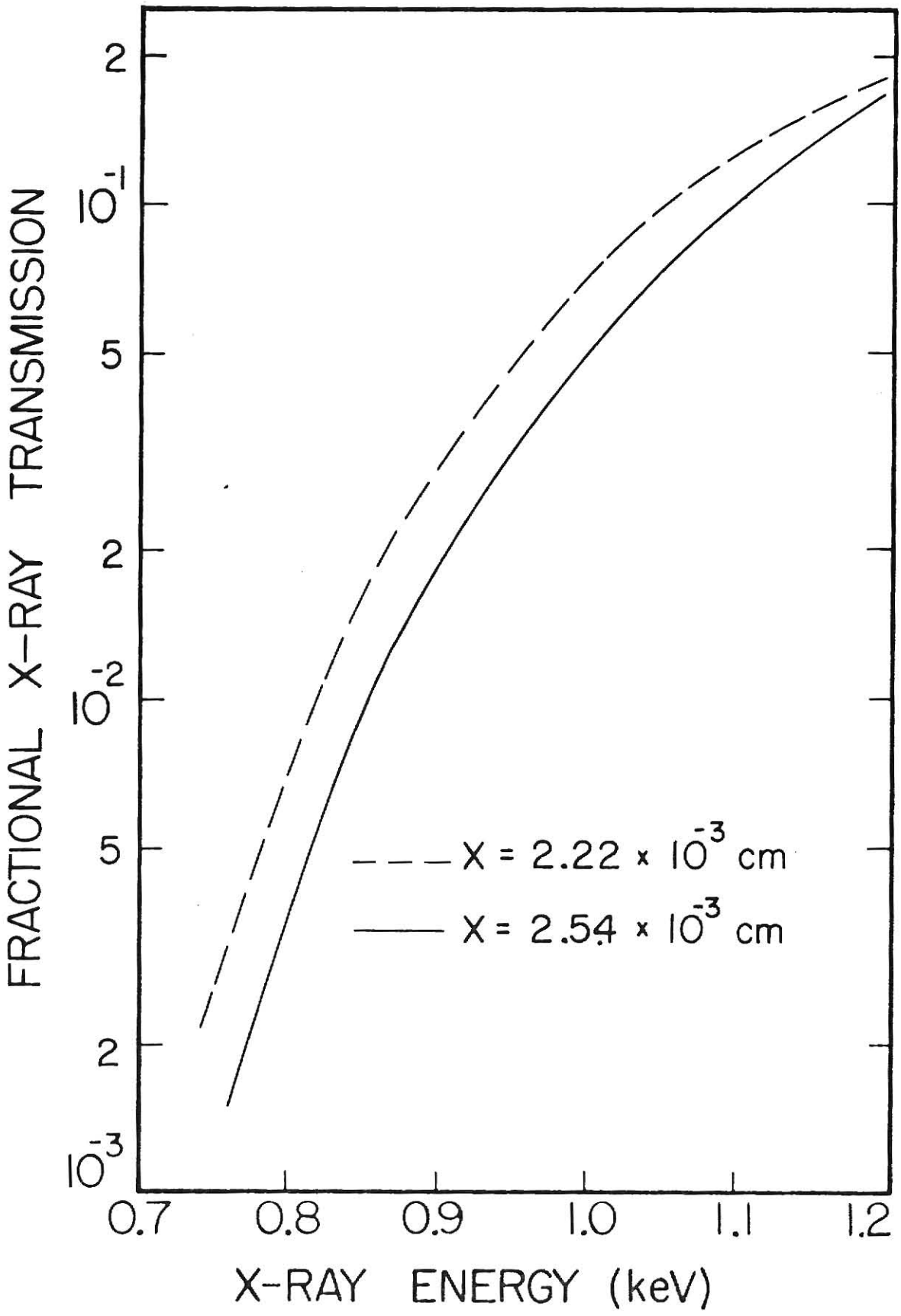
FRACTIONAL X-RAY TRANSMISSION
2
10^{-1}
5
2
10^{-2}
5
2
10^{-3}
0.7
0.8
0.9
1.0
1.1
1.2
X-RAY ENERGY (keV)
X = 2.22 x 10^{-3} cm
X = 2.54 x 10^{-3} cm

electronically by using an amplifier gating pulse, indicating the busy time in the analysis, to gate off the integration of the beam current. In this way the beam current was counted only during the time the detector amplifier was live. Count rates of up to 5000 x rays per second, with resulting dead time of up to 80% were used to test the accuracy of the correction procedure. In all cases, the electronic correction agreed within 10% of counting rates taken with a faster amplifier. During data accumulation for the actual experiment, the counting rate was always less than 1000 cts/sec (and usually much less) and the dead time correction never exceeded 20%. In the event of counting rates that were too high, the beam current was reduced. The corrected x-ray yields used include all such dead time corrections and the normalization procedure is estimated to be accurate to within 5%.

A sample x-ray spectrum obtained with fluorine 9+ ions passing through argon gas is shown in Plate VI. In deciding how to analyze such a spectrum, several options are open. The area of the entire peak, taken from limits set at the points where the peak fades into the background, can be integrated to give a total yield of observed x rays in the spectrum. Ordinarily this would permit x-ray production cross sections to be obtained, but with these x-rays from the fluorine projectiles, a choice must be made as to what detector efficiency to use to account for the x-ray absorption. Since the efficiency changes by almost an order of magnitude over the range of the peak from about 850 to 1100 eV, this choice is critical. Furthermore, the shoulder on the low energy side of the spectrum hints at the presence of more than one line. If one assumes that the spec-

Plate VI

Sample spectrum showing yield plotted as a function of channel number.

Plate VI

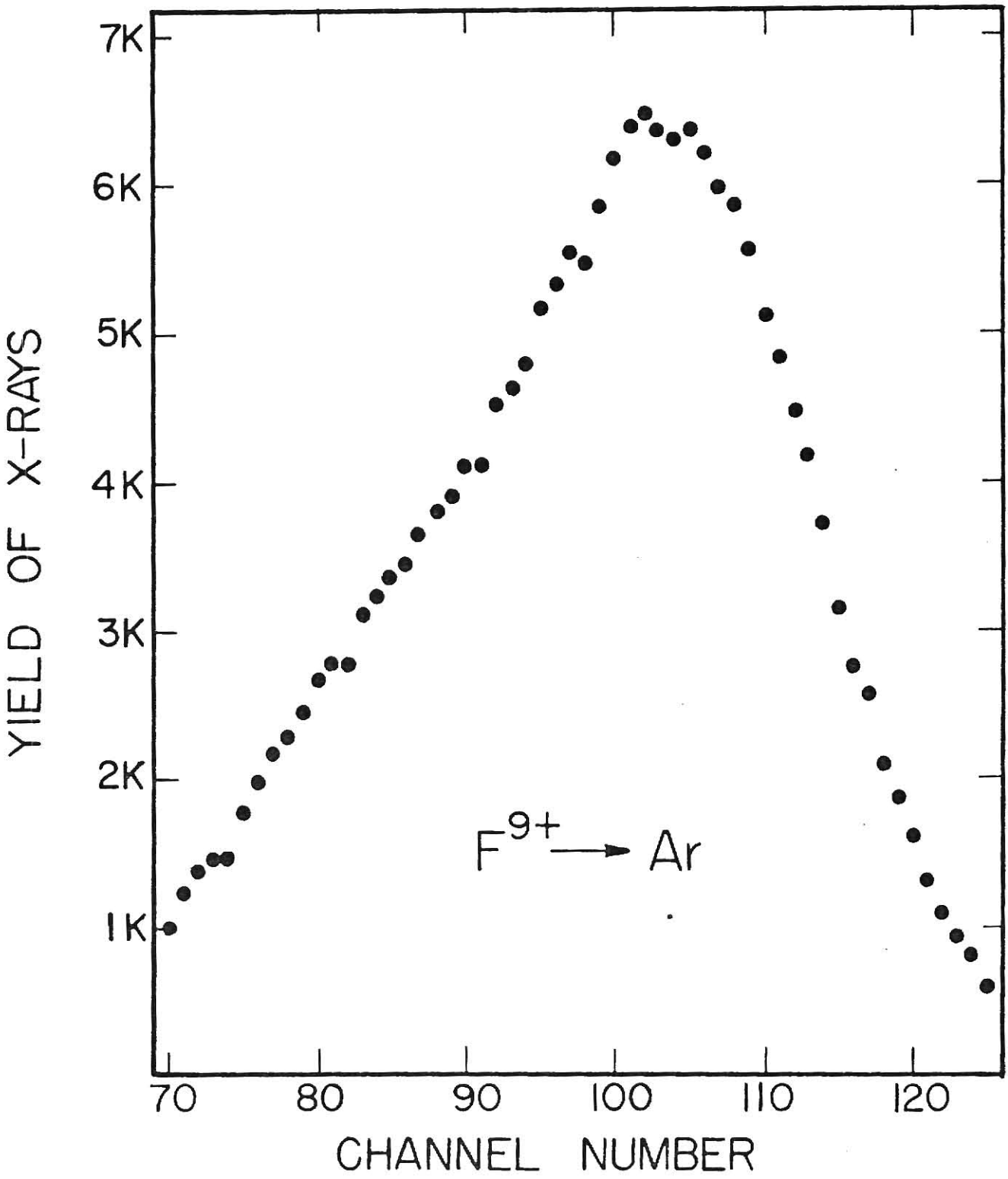
7K
6K
5K
4K
3K
2K
1K
YIELD OF X-RAYS
$F^{9+} \longrightarrow Ar$
70
80
90
100
110
120
CHANNEL NUMBER

trum contains just two lines, the efficiency for the lower energy line is much smaller than for the "main" line of the spectrum and one might suspect that the low energy shoulder corresponds to a line containing a very large number of x rays.

However, when one considers that the origin of the lines must be from electron capture to excited one-electron states, then one would expect the entire np-1s Lyman series to be present in the spectrum. The first of these occurs at 827 eV, the second at 980 eV, and the rest between approximately 1030 eV and 1100 eV (the series limit for the Lyman series is at 1103 eV), with the high energy lines being closer together than the low energy lines. The spectroscopy of this system has been investigated in a high resolution experiment[21] using a Bragg crystal spectrometer, and a sample spectrum of the fluorine Lyman series of x-rays is shown in Plate VII. Such a set of lines could fit the low resolution spectrum shown in Plate VII with the first line producing the shoulder (or lower peak) and the remaining lines, grouped close together, forming the main peak of the spectrum. It is important to note here that at such low energies (below 1 keV) the energy calibration of the solid state detector system is not necessarily linear because of the electronics of the analysis system. An x ray energy is converted to a voltage pulse which is digitized in an ADC. The nonlinearity in the digital representation of the x-ray pulse arises from a number of poorly understood complications such as the difference in DC levels of the DC coupled system and possible misadjustment of the time-to-peak setting of the internal gate of the analyzer. For a large voltage pulse (high energy x ray) this is only a small effect, but for the low energy x rays

Plate VII

High resolution spectrum from the experiment by Macdonald et al.[21]

Plate VII

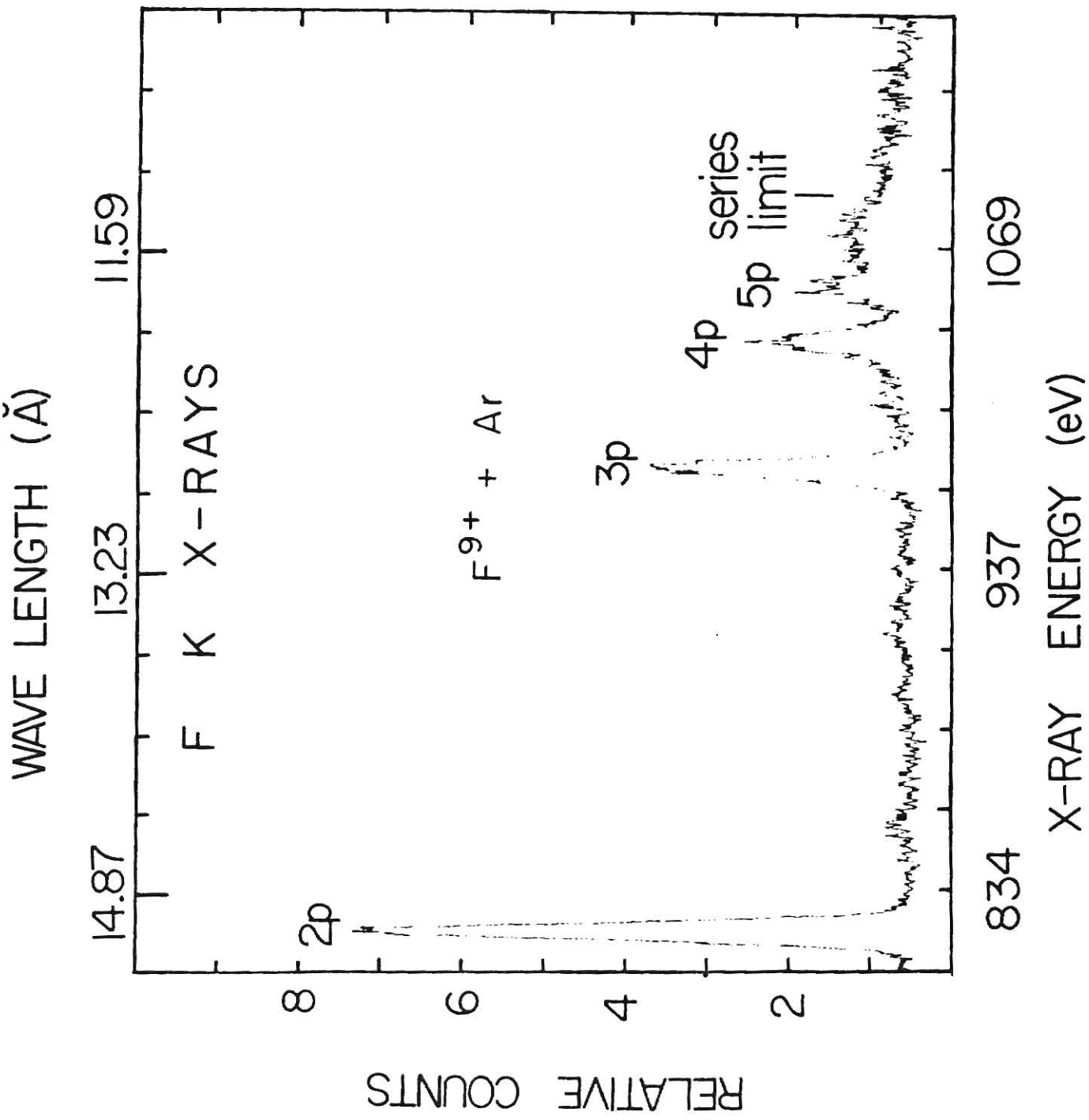
WAVE LENGTH (Å)
14.87
13.23
11.59
F K X-RAYS
F^{9+} + Ar
2p
3p
4p
5p
series limit
RELATIVE COUNTS
8
6
4
2
834
937
1069
X-RAY ENERGY (eV)

linearity is a significant source of error in the energy calibration. Thus the overlap of the lines on the spectrum may be slightly greater or less than a comparison of their energies would indicate.

To make the analysis of the spectra for the work of this thesis, a method was used based on the relative intensities of the lines observed under high resolution. The first four lines of the decay series were used assuming that the higher energy lines were negligibly small. Each line was spread into a gaussian peak and the resulting four peaks were added to produce a theoretical spectrum. In order to fit such a curve to the experimental spectrum, knowledge of the relative number of x rays in each line was considered essential in order to achieve a unique fit to the experimental data. The experiment done by Macdonald et al.[21] studying the same collision system by using a high resolution detection system (FWHM of about 2 eV), provided the crucial relative intensities. The results for the first four hydrogenic fluorine lines produced by electron capture by F^{9+} ions in argon normalized to the 2p-1s line are: 1.0, 0.26, 0.12, 0.08.

A computer program was used to calculate the required gaussians, compute the resulting curve, display the curve along with the data to be fit, and calculate a chi-square test for the fit (see Appendix I). The unknowns for the system included the peak positions, the peak width, the relative peak intensities following absorption in the detection system and an overall height multiplication factor (M) that permits normalization to the total number of x rays observed. The peak positions were theoretically known from the theoretical energy of each line, but due to the un-

cally known from the theoretical energy of each line, but due to the uncertain energy calibration of the analysis system in this energy region, they were varied within a limited range about their predicted values. The peak width was assumed to be the same for all peaks and was also varied around an initial value taken from the Ne K x-ray line produced by 3 MeV proton bombardment of a neon gas target during each run of these experiments. The relative peak intensities were initially fixed to the values obtained in a high resolution experiment, each line modified by the appropriate absorption of the Si(Li) detector for that energy. Then, these intensities were varied to see if this might improve the fit. By alternately varying one variable at a time and checking the resulting plot comparison and chi square test, the optimum values for the four peak positions, the peak width, the height multiplication factor (M) and a new set of normalized peak intensities slightly different from the original were obtained.

After extensive attempts to fit the data, it was found to be impossible to produce the low energy shoulder on the spectrum when the peak intensities remained fixed to their original values. By increasing the low energy line intensity, however, the final fit (Table II) was achieved. This implied that an intensity distortion occured somewhere in the system. The observed spectral shape can be altered or distorted by several different factors. For example, there is a low energy tail on all peaks measured by the Si(Li) detector which is not considered in this analysis. Although the magnitude of this tail is small, the assumption of a gaussian shape for the x-ray peaks may be responsible in part for the distortion of the spectrum. However, from previous experimental observations, the gaussian shape is

Table II

Final fit values for the four peak positions (given in channel numbers), the four relative peak heights (normalized), the peak width (FWHM), the pressures in microns for each run at that energy and the resulting intensity normalization factor (M). Some experimental runs were taken using a different total number of ions passing through the interaction region so that these results had to be normalized in order to obtain x-ray yield per micron pressure values. For 20.25 MeV, a fit was run for two different values of 2p-1s peak intensity (1.0 and 1.55). The numbers given with the energies are experimental run designations.

Table II

	Peak Positions (channels)				Peak Heights (normalized)				Peak Width (channels)	Pressures (microns Hg)	M	
	2P	3P	4P	5P	2P	3P	4P	5P			1.0	1.55
20.25 MeV (X1118)					1.0	1.37	.94	.73		3.74	68400	65500
										3.20	62500	61000
										3.10	42500	40600
					(1.55	1.37	.94	.73)		1.12	21500	20500
										.18	1780	1650
30 MeV (X2104)	82.3	99.8	105.8	109.5	1.0	1.37	.94	.73	21.3	4.62	49250	
										4.80	51400	
										2.74	30600	
										2.79	31050	
										.06	910	
										.06	875	
35.5 MeV (X2123)	82.5	101.0	105.0	110.0	1.0	1.37	.94	.73	21.3	3.14	23300	
										3.12	22700	
										4.92	14250	(35625)
										2.06	6400	(16000)
										.04	493	(1233)

normalized to 10K

probably a good approximation and cannot account for the inability to fit the main features of the spectrum.

The biggest factor involved in the distortion of the spectrum is the efficiency of transmission of the different x-ray lines into the detector. The relative intensities used in this analysis were calculated by attenuating the relative intensities from the high resolution experiment of Macdonald et al.[21] by an absorption factor approximately proportional to exp $(-axE^{-3})$ where x is the beryllium window thickness (known to within $\pm$ 20%). Because of the strong energy dependence within the exponential function, small variations in the thickness of the beryllium will dramatically change the relative intensities of the x-ray lines. Making the window thickness somewhat thinner results in a slightly weaker energy dependence for the efficiency. This means that the resulting attenuated relative peak intensities produce smaller high energy peaks or, alternatively, a bigger low energy shoulder. By varying the relative intensities in order to fit the shoulder of the observed spectrum and by comparing the increased magnitude of the low energy peak to each of the high energy peaks a new value for the window thickness was obtained. A good fit was obtained with a thickness Be of only 2.2×10^{-3}cm, only 13% less than the specified value of 2.5×10^{-3}cm. The dashed line on Plate V shows the transmission curve of the detector using this new window thickness.

For any one energy, the spectrum was largest and details of spectrum shape and proportion were clearest for experiments run at high target gas pressure. Therefore, the final values for all variables were fit to a high pressure run. Only M was changed to fit the remaining lower

pressure runs, since the other variables should remain constant at one energy for different target thicknesses. This assumption was checked in the course of the data fitting and no significantly better low pressure fits could be found. Final values of these variables for each energy are given in Table II. Excellent data fits were obtained for two energies (35.5 and 30.0 MeV) studied, but the fit for the third energy (20.25 MeV) was very poor (as discussed in the results section of this paper). Since there are a wide set of values that could produce such a poor fit, the actual values used to determine M were not considered significant.

It should be noted that, with six interdependent variables available, it is hard not only to locate the best fit, but also to estimate the errors inherent in the results of such a fit. The nonlinear energy calibration, responsible for four of these variables and the assumption that the peak widths were all the same, introduce an uncertainty in the intensity of the various x-ray lines. Another source of error in determining the proper distribution of the x-ray intensity arises from the gaussian distribution assumed for each peak. It is well established that Si(Li) detectors show a low energy tail which results in an asymmetric peak[34]. However, the biggest error involved with this method of analysis was the strong dependence of the efficiency of the detector for the different energy photons on the thickness of the Be window. A change of only 13% produced a big difference in efficiency; for example, at 827 eV the efficiency went from .006 to .011, at 981 eV from .04 to .06, at 1035 eV from .065 to .09 and at 1059 eV from .078 to .105. In this analysis, the calculated curves chosen to provide the height multiplication factor M was near enough to

the actual data curves so that M was known to within at least 3% and usually to within 1%. In the future, better results could be obtained by using a much thinner window. This would 1) significantly increase the efficiency and 2) decrease the energy dependence of the efficiency.

Plate VIII is a simple data fit spectrum in the final form. The total corrected yield "Y_t^c" needed for Eqn. (12) is given by:

$$Y_T^c = \sum_{i=1}^{4} 1/\xi_i \left[\frac{\Delta (M K_i)}{\Delta P} \right] \qquad (14$$

where i refers to the particular peak being considered (2p-1s, 3p-1s, ...), K_i is the relative intensity from the high resolution experiment[21], M is the overall multiplication factor, $\frac{\Delta MK_i}{\Delta P}$ is the slope of the intensity against pressure plot made for each x-ray peak, and ξ_i is the efficiency factor for each x-ray peak.

To complete the calculation for the x-ray production cross section (Eqn. 12), the target gas thickness (n') and the incident ion flux (N) must be calculated. The ideal gas law is sufficient to calculate the gas thickness (or number of atoms per unit volume) since the gas pressure was less than 10 microns of Hg. For a temperature of 20° C and a pressure of 1 micron Hg, (n') is equal to 3.293×10^{13} atoms/cm^3. The number of incident particles was measured by integrating the current on the last Faraday cup (see Plate III). The total projectile flux for each run was 1.389×10^{11} ions for the 20MeV and 35MeV runs, and 1.667×10^{11} ions for the 30MeV run.

Plate VIII

Sample plot of x-ray yield against detector channel number (a function of x-ray energy). The circles represent actual data points while the smooth line represents the fit to the data calculated by adding together four gaussian peaks.

Plate VIII

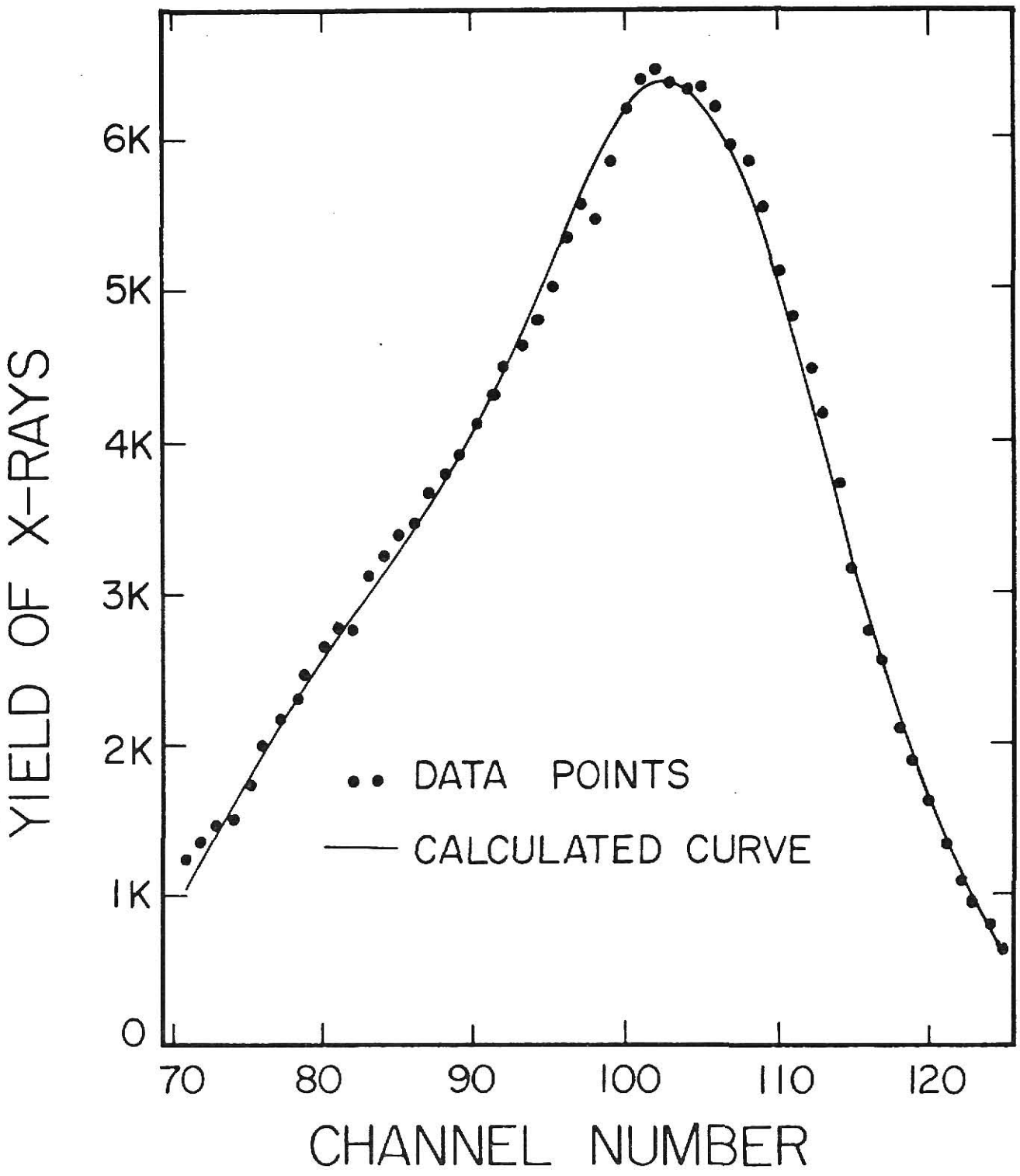
YIELD OF X-RAYS
6K
5K
4K
3K
2K
1K
0
70
80
90
100
110
120
CHANNEL NUMBER
DATA POINTS
CALCULATED CURVE

Results

In this work x-ray production cross sections have been measured for bare fluorine nucleii incident on argon gas at energies of 20, 30, and 35 MeV. These cross sections, along with the experimental cross sections for single electron capture to all states σ_c reported by Chiao[22] are plotted as a function of energy on Plate IX. A summary of this data is included in Table III. The cross sections for single electron capture to excited states σ_e are numerically equal to x-ray production cross sections since all of the captured electrons emit x rays while decaying to the ground state. However, some of these electrons may decay to the 2s state before going to the ground state. A final transition from 2s to 1s is not measured in this experiment due to several factors: 1) The 2s state is metastable with a lifetime of about 2.3×10^{-7} sec[35]. Since the fluorine projectile is within the interaction region for about 2×10^{-9} sec, very few 2s-1s transitions will occur within sight of the detector. 2) The most likely decay mode for a 2s-1s transition involves the release of two photons whose total energy is equal to the energy of the transition (E). Hence, the spectrum will be continuous and occur at energies too low to be seen by the detection system due to the extremely low efficiencies below $E \simeq 800$ eV. As a result the electron capture cross sections to excited states determined in this work (σ_e) do not include electron capture to or cascading to the 2s state.

The x-ray production cross sections given in Plate IX show a decreasing trend with increasing energy similar to the energy dependence of the electron capture cross sections. Table III includes the capture

Plate IX

Plot of cross sections as a function of incident projectile energy. Points connected by a smooth line are hydrogenic x-ray production cross sections of fluorine projectiles measured in this paper. Points connected by the dashed line are single electron capture cross sections measured by Chaio[22]. Lines are drawn only to guide the eye. The solitary circle represents the x-ray production cross section calculated with the 2p-1s relative intensity equal to 1.5.

Plate IX

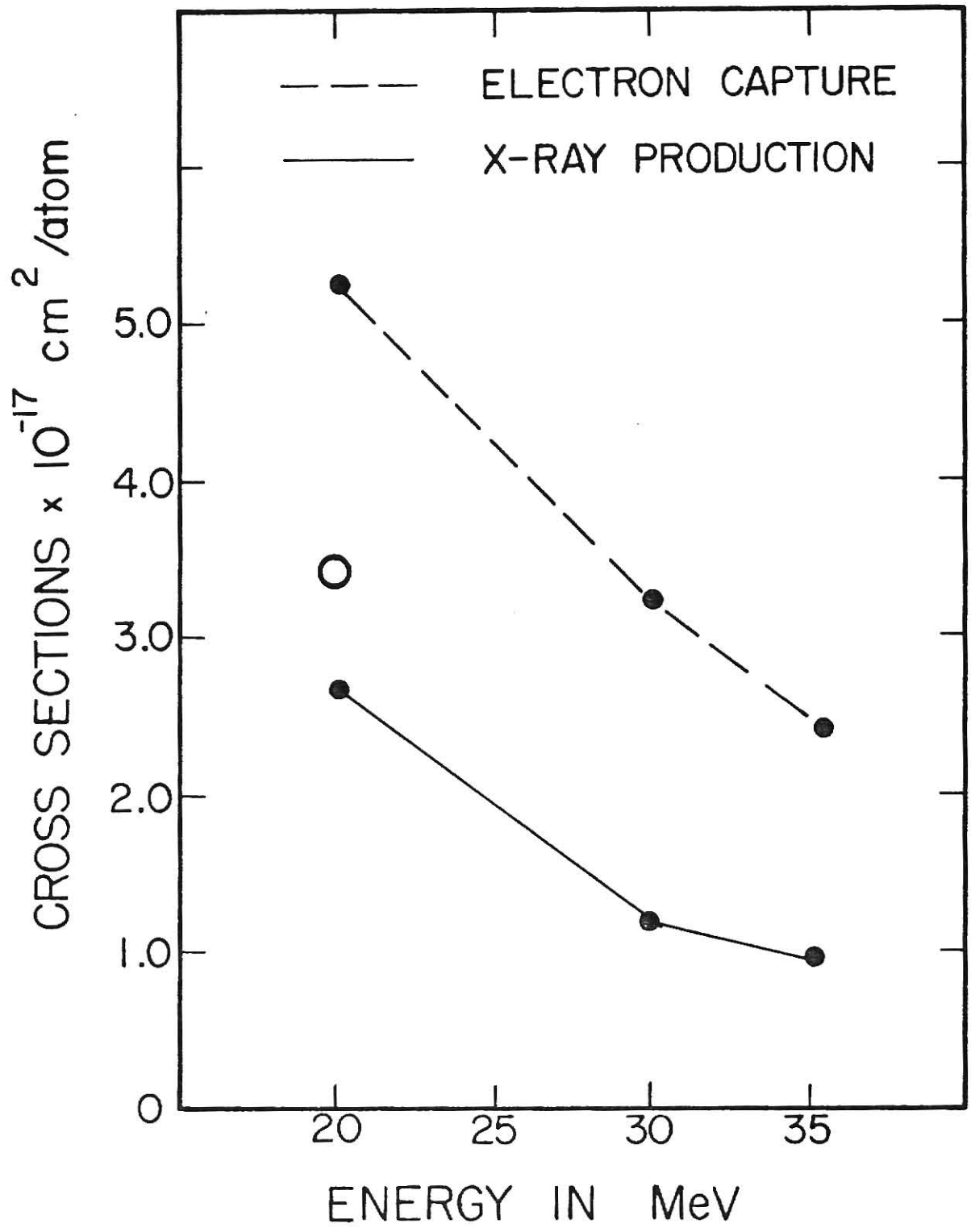
ELECTRON CAPTURE
X-RAY PRODUCTION
CROSS SECTIONS x 10^{-17} cm^2 /atom
5.0
4.0
3.0
2.0
1.0
0
20
25
30
35
ENERGY IN MeV

Table III

X-ray production cross sections (σ_x) and single electron capture to all states[22] cross sections (σ_c) for three energies. The corresponding capture percentages (C) are also listed.

Table III

Energy Mev	Cross Sections $cm^2/atom$ $\sigma_x \times 10^{-17}$	$\sigma_c \times 10^{-17}$	C %
20.25	2.57	5.23	49%
30.0	1.20	3.25	37%
35.5	.947	2.46	38%

percentage C, defined as:

$$C = \sigma_e / \sigma_c \times 100 \qquad (15$$

The percentages range from 37% to almost 50%. Most electron capture theories[7-8] predict that electron capture is proportional to $1/n^3$ so that about 17% of the total electrons captured would be to excited states. Nikolaev[8], for example, has developed a closed form of the Brinkman-Kramers approximation for electron capture from any media (although for proton projectiles only). A $1/n^2$ model has also been suggested[9] and this would predict about 37% of the electrons captured are to excited states. Future experiments of this type would help in interpreting the relative magnitude of electron capture to excited states.

In order to obtain a rough approximation of what percentage of electrons captured to excited states are lost to the 2s state, a $1/n^2$ electron capture model may be assumed. In this model, each level captures a total number of electrons proportional to $1/n^2$ (levels 2-6 only) and these electrons were assumed to be distributed among the l states proportional to $(2l+1)$. Using this model and the branching percentages given on Plate I, the percentage of electrons ending up in the 2s state compared to the total captured to all excited states is about 14%. A second calculation done with capture permitted only to n levels 3,4,5 and 6 gives a percentage of 3.2%. Since the only contribution of the n=2 shell to 2s states is due to electrons initially captured to 2s, about 11% of the capture is directly to the 2s state in this model. According to this model then, the cross sections measured in this work comprise 86% of

the total capture cross sections to excited states and that most of the difference is due to capture directly to the 2s state (almost five times that due to decay to 2s). It should be emphasized here that this is only a tentative approximation taken from one out of many possible choices for models.

The major error in the determination of the cross sections in this work is from the efficiency of detection of the x rays. Since the efficiency was, in part, determined by the beryllium window thickness and the fitting technique and is also highly energy dependent, the error in the efficiency depends on a number of variables. For example, variations of up to 15% in the efficiency produce data fits that are quite close to the optimum fit. It is estimated that the error due to the efficiency is probably no more than 35%. Other errors include the manometer calibration (10%), solid angle correction (15%), charge state impurities in the incident ion beam (.5%), and statistics and data analyzing procedures (10%). The total error due to these factors is less than 21% (not including the error due to the efficiency).

The relative error between the cross sections taken at the two higher energies is considerably less than the absolute error since errors due to efficiency, solid angle, and manometer calibration can be ignored. The estimated relative error is less than 10% as long as the procedure used in this work for peak fitting is valid. However, the relative error for the data at 20 MeV may be as great as the absolute error. In fitting the spectra, the same efficiency and relative intensity values were used for all three incident ion energies. While good fits were obtained for 35 and 30 MeV, the 20 MeV spectrum proved impossible to fit (see Plate X).

Differing experimental conditions might be responsible for altering the spectrum shape although this is considered unlikely. Unless there is an x-ray energy shift because of a different satellite distribution at different incident ion energy there is no reason for the detector efficiency to change from 20 to 30 MeV. However, the problem is possibly due to a difference in initial relative intensity in the excited state distribution. Since the relative intensities reported by Macdonald et al.[21] were taken at 35 MeV, the relative intensities at an energy 15 MeV lower might be different due to a difference in the distribution of captured electrons among the excited states. As single electron capture to all states is energy dependent, this is a reasonable cause for this variation. A good fit was achieved by increasing the 2p-1s relative intensity from 1.0 to 1.5 and the resulting cross section is displayed in Plate IX as the open circle. Its value is 20% higher than the result obtained by keeping the intensity ratios fixed.

It is suggested that future experiments of this type be conducted with either a much thinner detector window or in a different photon energy range in order to reduce the errors due to the efficiency. A wider range of incident energies should also be used to 1) test whether the decrease in cross sections with increase in incident energy is a general phenomenon and 2) check the dependence of the capture percentage C on the incident energy.

Plate X

Sample plot of x-ray yield against detector channel number (a function of x-ray energy) for 20 MeV fluorine ions. The circles represent actual data points while the smooth line represents the fit to the data calculated by adding together four gaussian peaks. The low shoulder was not possible to fit without changing the relative intensity of the 2p-1s transition.

Plate X

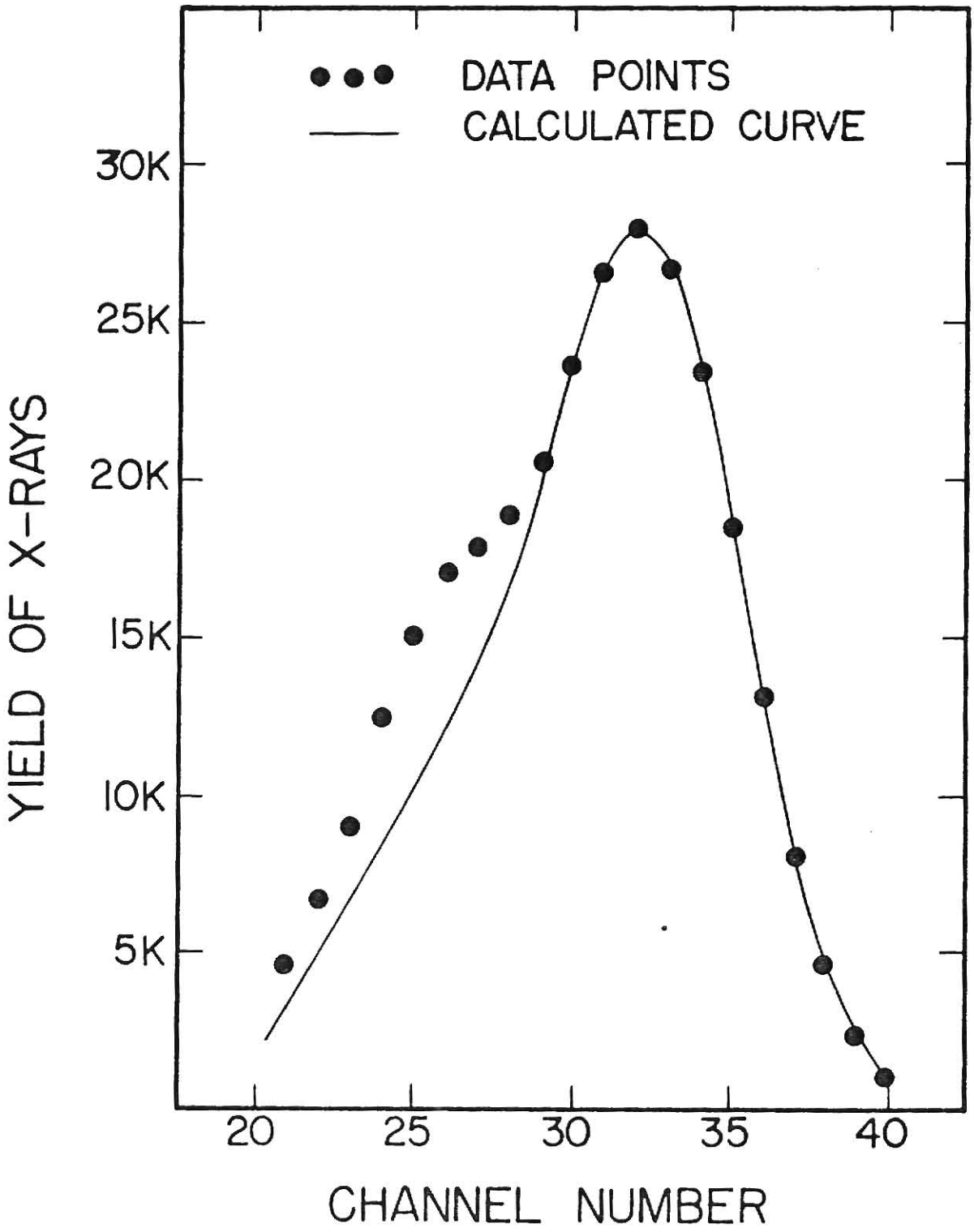
DATA POINTS
CALCULATED CURVE
30K
25K
20K
15K
10K
5K
YIELD OF X-RAYS
20
25
30
35
40
CHANNEL NUMBER

Conclusion

X-ray production cross sections for hydrogenic decay in fluorine resulting from fully stripped fluorine ions incident on argon gas are reported here for three incident energies. Ignoring effects of capture and decay to the 2s state, these cross sections are numerically equal to cross sections for single electron capture to excited states. When compared with total single electron capture (to all states) these cross sections are found to be from 37% to 50% of the total, thus showing that a larger percentage of electrons are captured to excited states than is predicted by a $1/n^3$ model.

Acknowledgements

The author would like to thank Dr. Matt Brown, Loren Winters, Tang Chaio, and Dr. L. Ellsworth for their help in taking experimental data and, in particular, Dr. J. R. Macdonald for assistance with the experiment and especially for his invaluable advice and encouragement in the preparation of this thesis. The author also gratefully acknowledges support from the Atomic Energy Commission and the Department of Physics, Kansas State University and its faculty and support services.

References

1. J. D. Garcia, R. J. Fortner, and T. M. Kavanagh, Rev. Mod. Phys. 45, 111 (1973).

2. U. Fano and W. Lichten, Phys. Rev. Lett. 14, 627 (1965); W. Lichten, Phys. Rev. 164, 131 (1967).

3. H. D. Betz, Rev. Mod. Phys. 44, 465 (1972).

4. E. J. McGuire, Phys. Rev. A 3, 587 (1971).

5. H. D. Betz and A. B. Wittkower, Phys. Rev. A 6, 1485 (1972).

6. I. S. Dmitriev and Y. A. Teplova, JETP 34, 1485 (1972).

7. J. R. Oppenheimer, Phys. Rev. 31, 349 (1928).

8. V. S. Nikolaev, JETP 24, 847 (1967).

9. K. Omidvar, Phys. Rev. Lett. 30, 941 (1973).

10. I. A. Sellin, B. L. Donnally, and C. Y. Fan, Phys. Rev. Lett. 21, 717 (1968); I. A. Sellin, M. D. Brown, W. W. Smith, and B. L. Donnally, Phys. Rev. A, 2, 1189 (1970).

11. R. W. Schmieder and R. Marrus, Phys. Rev. Lett. 25, 1245 (1970); R. Marrus and R. W. Schmieder, Phys. Rev. Lett. 25, 1689 (1970).

12. C. L. Cocke, B. Curnutte, and J. R. Macdonald, Phys. Rev. Lett. 28, 1233 (1972).

13. P. Richard, R. L. Kauffman, F. F. Hopkins, C. W. Woods, and K. A. Jamison, Phys. Rev. Lett. 30, 888 (1973).

14. T. M. Kavanagh, M. E. Cunningham, R. C. Der, R. J. Fortner, J. M. Khan, E. J. Zaharis, J. D. Garcia, Phys. Rev. Lett. 25, 1473 (1970).

15. L. Winters, J. R. Macdonald, M. D. Brown, L. D. Ellsworth, T. Chiao, and E. W. Pettus "Chlorine K X-Ray Production in Collisions of Chlorine ions with Gas Targets" in Electronic and Atomic Collision, Abstracts of Papers VIII ICPEAC, (Institute of Physics, Beograd, Yugoslavia) Vol. II, p. 741 (1973).

16. H. Kubo, F. C. Jundt, and K. H. Purser, Bull. Am. Phys. Soc. 18, 559 (1973); and submitted for publication.

17. S. Datz, C. D. Moak, B. R. Appleton, and T. A. Carlson, Phys. Rev. Lett. 27, 363 (1971).

18. C. W. Woods, Forrest Hopkins, Robert L. Kauffman, D. O. Elliott, K. A. Jamison, Patrick Richard, Phys. Rev. Lett. 31, 1 (1973).

19. H. J. Stern, H. O. Lutz, P. H. Mokler and P. Armbruster, Phys. Rev. A 5, 2126 (1972).

20. C. L. Cocke, R. Randall and B. Curnutte, "Impact Parameter Dependence of Chlorine K X-Ray Production in Violent Cl-Al, Cl-Ti and Cl-Cu Collisions" in Electronic and Atomic Collision, Abstracts of Papers VIII ICPEAC, (Institute of Physics, Beograd, Yugoslavia) Vol. II, p. 714 (1973).

21. J. R. Macdonald, P. Richard, C. L. Cocke, M. D. Brown and I. A. Sellin, Phys. Rev. Letters (submitted for publication).

22. T. Chiao, Ph.D. Thesis.

23. H. C. Brinkman and H. A. Kramers, Proc. Acad. Sci. Amsterdam 33, 973 (1930).

24. D. P. Bates and R. McCarrol, Adv. in Phys. 11, 39 (1962); A. Dalgarno, in Atomic and Molecular Processes, edited by M. R. McDowell (North Holland Publ. Co. Amsterdam), p. 609 (1964).

25. J. D. Jackson and H. Schiff, Phys. Rev. 89, 359 (1953).

26. H. Schiff, Can. J. Phys. 32, 393 (1954).

27. N. Bohr and J. Lindhard, Kgl. Danske Videnskab Selskab Mat.-Fys. Medd, 28, No. 7 (1954).

28. W. L. Wiese, M. W. Smith, B. M. Glennon, NSRDS-NBS 4, Vol. 1 (1966).

29. Kevex Corporation, Burlingame, California.

30. Hewlett-Packard Calculator, Model 9100B, Program Library.

31. W. J. Veigele, Atomic Data Tables 5, 51 (1973).

32. R. L. Watson, L. W. Lewis and J. B. Nalowitz, Nucl. Phys. A, 154, 561 (1970).

33. R. J. Gehrke and R. A. Lakkan, Nucl. Instrum. Methods, 97, 219 (1971).

34. L. M. Winters, J. R. Macdonald, M. D. Brown, L. D. Ellsworth, and T. Chiao, Phys. Rev. A, 7, 1276 (1973).

35. W. R. Johnson, Phys. Rev. Lett, 29, 1123 (1972).

Definition of Symbols

Z_1	atomic number of projectile ion
Z_2	atomic number of target atom
n	principle quantum number
Ω	solid angle correction factor seen by the detector from an arbitrary point
$\mathcal{L}$	interaction length of the beam line
σ	x-ray production cross section in cm^2
N	number of incident particles
n'	number of target atoms per unit volume at one micron of Hg pressure at 20° C
Y_T^c	total x-ray yield per micron of pressure corrected for 1) detector efficiency and 2) electronic dead time
Ω_T	$\Omega \mathcal{L}$ total solid angle correction factor
σ_c	cross section for capture of one electron to any state
σ_e	cross section for capture of one electron to any excited state
C	σ_e/σ_c x 100 capture percentage
M	overall multiplication factor which converts normalized x-ray intensities to actual x-ray intensities.

APPENDIX

A COMPUTER PROGRAM

```
C       GAUSC  TO BE USED WITH PLTC AND SYMC
C       A PROGRAM TO TAKE INPUT INFORMATION AND CONSTRUCT FOUR
C       GAUSIAN PEAKS, ADD THEM TOGETHER AND DISPLAY THE
C       RESULTING CURVE ALONG WITH A DATA SPECTRUM.
C       AN UNNORMALIZED CHI SQUARED CALCULATION IS ALSO MADE.
C       THE GAUSIANS ARE DEFINED BY THESE VARIABLES:
C
C       M=OVERALL MULTIPLICATION FACTOR
C       FWHM=FULL WIDTH HALF MAXIMUM
C       H2P=RELATIVE INTENSITY FOR 2P-1S TRANSITION (LOWEST ENERGY)
C       H3P=     "          "     " 3P-1S     "          "     "
C       SIMILAR FOR H4P AND H5P
C       C2P THRU C5P ARE SIMILAR TO ABOVE EXCEPT THEY REFER TO
C           PEAK POSITION CHANNELS .
C
C       OTHER PROGRAM VARIABLES INCLUDE:
C
C       FILE=THE FILE # (DO NOT INCLUDE BIN)
C       SPEC=SPECTRUM #
C       SIZE=# CHANNELS IN SPECTRUM
C       LO=LOWER LIMIT FOR SPECTRUM DISPLAY AND CHI SQUARED CALC.
C       HI=UPPER LIMIT (AS FOR LO)
C       LPVAL=DISPLAY VARIABLE; =0 FOR DISPLAY ON SCOPE,=1 FOR
C           DISPLAY ON LINE PRINTER, =2 FOR NO DISPLAY
C       FCNG=DISPLAY VARIABLE; =0 IGNORE, =1 GO TO HEAD OF
C           PROGRAM FOR A NEW FILE, =2 DISPLAY CURRENT VALUES OF
C           ALL VARIABLES ON TELETYPE
C
C       TO USE:  LOAD PROGRAMS OGAUSC,SYMC,PLTC
C           (NOTE:  MONITOR TAPE MUST HAVE KELLER'S READER PROGRAM
C           ON IT; FOR EXAMPLE, USE EXTENDED MONITOR)
C       SELECT FILE #, AFTER VARIABLES ARE PRINTED OUT,CHANGE ANY
C           REQUIRED BY TYPING FOR EXAMPLE (FWHM=20;), HIT ALT
C           KEY WHEN DONE AND PROGRAM WILL EXECUTE.
C
      REAL M,H,C,Y,PI,D,SIG,DEM,MAX,TH
      REAL *FILE(2),FWHM,CURVE,KISQ,SKISQ
      REAL H2P,H3P,H4P,H5P,C2P,C3P,C4P,C5P,PHI2,PHI3,PHI4,PHI5
      REAL SQRT,EXP,AMAX1
      INTEGER TT,LP,DT,LO,HI,I,J,K,X,VP,LPVAL
      INTEGER DATA,BASE,SIZE,SPEC,FCNG
      LOGICAL FOUND,PASS2
      COMMON DATA(4096)
      DATA TT,LP,DT,PI,M/1,2,3,3.14159,1.0/,VP,LPVAL/8,0/
      DATA H2P,H3P,H4P,H5P/1.0,1.37,.94,.73/
      DATA C2P,C3P,C4P,C5P/81.5,101.0,105.0,110.0/
      DATA LO,HI,FWHM,SIZE/70,124,21.3,1024/,FCNG/0/
      DATA FILE(2)/4H BIN/,FILE(1),SPEC/5HX2113,1/
C
      F(H,C)=M*H*(EXP(-(C-Y)*(C-Y)/(2.0*SIG*SIG)))/DEM
C
      CALL SYMC(FCNG,SPEC,SIZE,LO,HI,FWHM,M,H2P,H3P,H4P,H5P,
     1    C2P,C3P,C4P,C5P,LPVAL,TH)
C
1002  WRITE(TT,502)
502   FORMAT(14H FILE NAME, A5)
      READ(TT,602)FILE(1)
602   FORMAT(A5)
```

```
      CALL FSTAT(DT,FILE,FOUND)
      IF(FOUND)GO TO 109
      WRITE(TT,405)FILE
405   FORMAT(6H FILE ,A5,,4,10H NOT FOUND)
      GO TO 102
109   CALL SEEK(DT,FILE)
      DO 99 I=1,4096,64
      J=I+63
99    READ(DT) (DATA(K),K=I,J)
      CALL CLOSE(DT)
C
C     INPUT
C
101   LPVAL=0
      FCNG=0
      WRITE(TT,501)SIZE,LO,HI,FWHM,M,H2P,H3P,H4P,H5P,
     1    C2P,C3P,C4P,C5P,FILE,SPEC,LPVAL,FCNG
501   FORMAT(21H DEFAULT VALUES ARE:,/8H SIZE = ,I4,4X,
     1    9H LO,HI = ,2(I4,1X),10H   FWHM = ,F6.2,7H   M = ,F12.3/
     2    11H H2P-H5P = ,4(F7.3),1X,11H C2P-C5P = ,4(F6.1,1X)/
     3    6H FILE = ,A5,A4,2X,8H SPEC = ,I2/
     4    9H LPVAL = ,I1,18H (LP=1,VP=0,NON=2)
     5    8H FCNG = ,I1,32H (NEW FILE=1,  DISPLAY VALUES=2))
C
105   CALL READER(3H OK)
      IF(1-FCNG)1,1,102,104
104   IF(LPVAL.EQ.1)CALL LPCTL (6,-88,2)
C
C
C     TEST
C
      I=64
      DO 10 J=1,7
      IF(I.EQ.SIZE)GO TO 20
10    I=2*I
      WRITE(TT,401)SIZE
401   FORMAT(11H ERROR SIZE = ,I4)
      GO TO 101
20    IF(SPEC.GE.1.AND.SPEC*SIZE.LE.4096)GO TO 30
      WRITE(TT,402)SIZE,SPEC
402   FORMAT(24H ERROR SIZE OR SPEC NO. ,2I4)
      GO TO 101
30    A=LO
      B=HI
      S=SIZE
      IF(A.LT.C2P.AND.C5P.LT.B.AND.B.LE.S)GO TO 40
      WRITE(TT,403)LO,HI,C2P,C3P,C4P,C5P
403   FORMAT(23H ERROR LIMITS OR POSITIONS  ,2I4,2X,4(F8.2,1X))
      GO TO 101
40    IF(C2P.LT.C3P.AND.C3P.LT.C4P.AND.C4P.LT.C5P)GO TO 130
      WRITE(TT,404)C2P,C3P,C4P,C5P
404   FORMAT(21H ERROR IN POSITIONS  ,4(F8.2,1X))
      GO TO 101
C
C     PROGRAM INITIALIZATION
C
130   PASS2=.FALSE.
      PAY=1.0
```

```
131     SKISQ=0.0
        X=LO-1
        SIG=FWHM/2.3548
        DEM=SIG*SQRT(2.0*PI)
C
C       PROGRAM
C
        DO 140 I=1,1000
        X=X+1
        Y=X
        PHI2=F(H2P,C2P)
        PHI3=F(H3P,C3P)
        PHI4=F(H4P,C4P)
        PHI5=F(H5P,C5P)
        CURVE=PHI2+PHI3+PHI4+PHI5
C
        BASE=SIZE*(SPEC-1)
        J=BASE+X
        D=DATA(J)
        KISQ=(CURVE-D)*(CURVE-D)
        SKISQ=SKISQ+KISQ
        MAX=AMAX1(MAX,D,CURVE)
C
132     IF(PASS2)CALL PLTC(CURVE,D,MAX,X,LPVAL)
        IF(X.GE.N))GO TO 700
140     CONTINUE
C
        IF(LPVAL.EQ.2)GO TO 103
700     IF(PASS2)GO TO 100
        PASS2=.TRUE.
        IF(LPVAL.NE.1)GO TO 103
C
        WRITE(LP,704)FILE,SPEC
704     FORMAT(1H1 10H FILE NO. ,A5,A4,4X,14H SPECTRUM NO. ,I2/)
        WRITE(LP,701)LO,HI,FWHM,M,C2P,C3P,C4P,C5P
701     FORMAT(24H LIMITS OF SPECTRUM ARE ,I4,I4,6X,
     1     6H FWHM = ,F6.2,6X,25H MULTIPLICATION FACTOR = ,F12.3/
     2     23H PE/K POSITIONS 2P-5P  ,4(F7.2,2X))
        WRITE(LP,705)H2P,H3P,H4P,H5P,SKISQ
705     FORMAT(30H RELATIVE PEAK HEIGHTS 2P-5P  ,4(F7.3,1X)/
     1     15H CHI SQUARED = ,E12.6//
     2     19H CHAN  CURVE   DATA/)
        GO TO 131
C
103     WRITE(TT,702)SKISQ
702     FORMAT( 15H CHI SQUARED = ,E12.6/)
        IF(LPVAL.EQ.2)GO TO 100
        WRITE(VF,703)SKISQ
703     FORMAT(1H1 )5H CHI SQUARED = ,E12.6)
        GO TO 131
        STOP
        END
```

```
PAGE    1       SYMC    SRC

     1                                      SUBROUTINE SYMC
     2                                      INTEGER 'FCNG'
     3                                      INTEGER 'SPEC'
     4                                      INTEGER 'SIZE'
     5                                      INTEGER 'LO'
     6                                      INTEGER 'HI'
     7                                      REAL 'FWHM'
     8                                      REAL 'M'
     9                                      REAL 'H2P'
    10                                      REAL 'H3P'
    11                                      REAL 'H4P'
    12                                      REAL 'H5P'
    13                                      REAL 'C2P'
    14                                      REAL 'C3P'
    15                                      REAL 'C4P'
    16                                      REAL 'C5P'
    17                                      INTEGER 'LPVAL'
    18                                      REAL 'TH'
    19                                      RETURN
    20                                      END
                SIZE=00076      NO ERROR LINES
```

```
C       SUBROUTINE PLTC   FOR GAUSC
C
        SUBROUTINE PLTC(C,D,MAX,X,LPV)
C
        REAL C,D,MAX,L.NE(45),LIN(123),BLANK,CSYM,DSYM
        INTEGER LP,VP,X.I,J,K,WID,LPV,ID,IC,ICURV,IDAT
        DATA LP,VP/2,8/
        DATA BLANK,CSYM,DSYM/1H ,1HC,1H*/
C
        IF(LPV.EQ.1)GO TO 121
        WID=45
        DO 120 K=1,WID
120     LINE(K)=BLANK
        GO TO 123
121     WID=103
        DO 122 K=1,WID
122     LIN(K)=BLANK
C
123     ID=D
        IC=C
        ICURV=C
        IDAT=D
C
130     IF(ID-WID)140,131,131
131     ID=ID/10
        GO TO 130
140     IF(IC-WID)150,141,141
141     IC=IC/10
        GO TO 140
150     IF(IC)151,151,152
151     IC=1
152     IF(ID)153,153,154
153     ID=1
C
154     IF(LPV.EQ.1)GO TO 160
        LINE(IC)=CSYM
        LINE(ID)=DSYM
        WRITE(VP,501)X,ICURV,IDAT,(LINE(K),K=1,WID)
501     FORMAT(I5,I6,I6,45A1)
        RETURN
C
160     LIN(IC)=CSYM
        LIN(ID)=DSYM
        WRITE(LP,502)X,ICURV,IDAT,(LIN(K),K=1,WID)
502     FORMAT(I5,I7,1X,I6,103A1)
        RETURN
        STOP
        END
```

PROJECTILE X-RAY CROSS SECTIONS FOR FULLY STRIPPED FLUORINE IONS ON ARGON

by

EDWARD WILLIAM PETTUS JR.

B.S., Purdue University, 1971

AN ABSTRACT OF A MASTER'S THESIS

submitted in partial fulfillment of the

requirements for the degree

MASTER OF SCIENCE

Department of Physics

KANSAS STATE UNIVERSITY
Manhattan, Kansas

1974

PROJECTILE X-RAY CROSS SECTIONS FOR FULLY STRIPPED FLUORINE IONS ON ARGON

Fluorine x-ray yields were measured as a result of fully stripped fluorine projectiles incident on argon gas at incident projectile energies of 20, 30 and 35 MeV. X-ray yields as a function of argon gas pressure under single collision conditions were measured with a Si(Li) x-ray detector. The resulting x-ray spectrum was resolved and analyzed using previous high resolution data and computer techniques assuming single electron capture to an excited state and the resultant radiative decay. The x-ray production cross sections were compared with single electron capture cross sections and a percentage of single electron capture to excited states was obtained that was significantly higher than the usual $1/n^3$ model would predict.